BULLETIN OF THE POLISH ACADEMY OF SCIENCES
TECHNICAL SCIENCES
Vol. 57, No. 4, 2009
DOI: 10.2478/v10175-010-0135-y

Control and modulation methods of voltage source converter

G. RADOMSKI*

Power Electronics Department, Kielce University of Technology, 7 Tysiąclecia Państwa Polskiego Ave, 25-314 Kielce, Poland

Abstract. Control and modulation methods of Voltage Source Converter (VSC) have been presented in the paper. Model of VSC with three value transistor branch state function is introduced to describe operation of VSC. Predictive-corrective control method of VSC system is presented. Two variants of Space Vector PWM methods for VSC system are developed. Algorithm of cancelation of negative influence of dead time on the AC voltages is implemented in the proposed modulation methods. Correctness of introduced method is validated by simulation and experiment investigations.

Key words: power converters, voltage source converter, predictive control, space vector PWM.

Notation

ω	–	angular frequency of the mains,
T	–	control and modulation period,
R	–	input choke resistance,
L	–	input choke inductance,
R_o	–	load resistance,
R_{TD}	–	output resistance of inactive converter transistor-diode branch (both transistor switched off and branch current value of zero),
U_{RMS}	–	RMS value of phase voltage,
u_{Sin}, u_{San}, u_{Sbn}, u_{Scn}	–	AC converter voltages referenced to the mid point of the output voltage,
u_{Si}, u_{Sa}, u_{Sb}, u_{Sc}	–	AC converter voltages referenced to the neutral point of the mains,
u_{Nn}	–	voltage between mid point of output voltage and neutral point of the mains,
u_{S0}	–	zero component of the mains voltage,
r_{Si}	–	output resistance of converter transistor branch,
i_i, i_a, i_b, i_c	–	phase currents,
S_i, S_a, S_b, S_c	–	state functions of transistor branch,
s_{ip}, s_{ap}, s_{bp}, s_{cp}	–	state functions of high side transistor of converter branch,
s_{in}, s_{an}, s_{bn}, s_{cn}	–	state functions of low side transistor of converter branch,
i_{pi}, i_{pa}, i_{pb}, i_{pc}	–	currents delivered to positive output rail,
i_{ni}, i_{na}, i_{nb}, i_{nc}	–	currents delivered to negative output rail,
u_{dc}	–	output DC voltage of the converter system,
i_{dcin}	–	input current of DC circuit,
i_{dcout}	–	output current of DC circuit,
i_C	–	current of DC circuit capacitor,
$\mathbf{C}_{n\rightarrow\alpha\beta}$	–	conversion matrix from 3 to 2 phase stationary reference frame,
$\mathbf{u}_{S\alpha\beta}$	–	AC voltage space vector,
$\underline{V}_{Sdq}$	–	AC voltage space vector in synchronously rotated reference frame,
$\underline{V}_{dq}$	–	voltage space vector of the mains in synchronously rotated reference frame,
$\underline{I}_{dq}$	–	current space vector in synchronously rotated reference frame,
$\underline{V}_{d}$	–	shift vector,
$\underline{V}_{dI}$, $\underline{V}_{dI3}$, $\underline{V}_{dI4}$	–	current component of shift vector,
$\underline{V}_{dV}$, $\underline{V}_{dV3}$, $\underline{V}_{dV4}$	–	voltage component of shift vector,
$\underline{V_{Sp}}$, $\underline{V_{SpdI}}$, $\underline{V_{SpdIV}}$	–	vector signals of feedback path for predictive control algorithm,
$\underline{\mathbf{V}}_{(\mathbf{i})dq}$	–	voltage space vector of the mains calculated on the basis of measurements,
$\underline{\mathbf{I}}_{(\mathbf{i})dq}$	–	current space vector calculated on the basis of measurements,
$\underline{\Delta\mathbf{I}}_{(\mathbf{i})dq}$	–	regulation error of current space vector,
$\underline{\mathbf{V}}_{S(\mathbf{i})dq}$	–	converter AC voltage space vector calculated in the previous step,
$\underline{\tilde{\mathbf{I}}}_{(i+1)dq}$	–	current space vector predicted on the basis of measurements of current step and converter AC voltage calculated in the previous step,

*e-mail: radomski@tu.kielce.pl

$\Delta\tilde{\underline{\mathbf{I}}}_{(i+1)dq}$ – regulation error of predicted current space vector,
$\tilde{\underline{\mathbf{V}}}_{(i+1)\alpha\beta}$, $\tilde{\underline{\mathbf{V}}}_{(i+1)dq}$ – voltage space vector of the mains predicted for the next step,
$\underline{\mathbf{I}}_{dq\ ref}$ – reference current space vector,
$\underline{\mathbf{V}}_{S(i+1)dq}$ – voltage space vector calculated for the next step,
T_d – dead time,
$SectI$ – current sector number,
$SectV$ – voltage sector number.

1. Introduction

Two level Voltage Source Converter is a standard application widely used in industry as a rectifier, inverter and compensator system. This application is chosen as basic by leading world electrical companies for its efficiency and simplicity. Although it is regarded as a well known and established system, there are still some aspects worth analysing. Concurrently to multilevel converter systems development the high precision control and modulation systems of two level VSC are still considered [1–8]. It is due to its simplicity and high efficiency.

1.1. Model of voltage source converter. The connection diagram of VSC system is illustrated in Fig. 1. A transistor-diode matrix of VSC is modelled by cross-coupled, controlled voltage and current sources [8]. The equivalent connection diagram is presented in Fig. 2.

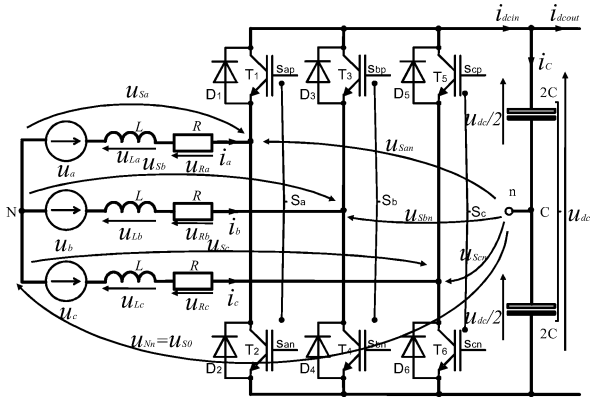

Fig. 1. Three phase voltage source converter

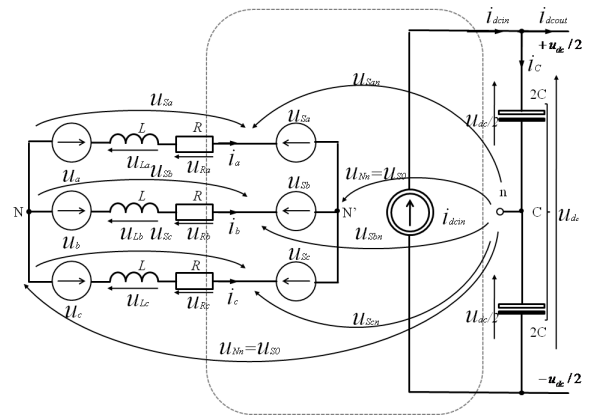

Fig. 2. Three phase voltage source converter equivalent circuit

Three value transistor branch state function (5) and three level current sign function are used in the model of converter.

Voltage of one converter branch is described by (1) while its internal resistance by (2):

$$u_{Sin} = \left[S_i + (1 - |S_i|)\, sign\,(i_i)\right] \frac{u_{dc}}{2}, \tag{1}$$

$$r_{Si} = (1 - |S_i|)\,(1 - |sign(i_i)|)\, R_{TD}. \tag{2}$$

The current that is delivered to the positive output rail is described by (3).While the current is delivered to the negative output rail is described by (4):

$$i_{pi} = \left[\frac{S_i + 1}{2}\,|S_i| + (1 - |S_i|)\,\frac{sign\,(i_i) + 1}{2}\right] i_i, \tag{3}$$

$$i_{ni} = \left[\frac{S_i - 1}{2}\,|S_i| + (1 - |S_i|)\,\frac{sign\,(i_i) - 1}{2}\right] i_i, \tag{4}$$

where $i \in \{a, b, c\}$ and transistor branch state function is defined by (5).

$$S_i \in \{-1,\, 0,\, 1\}, \quad \begin{cases} S_i = 1 \Leftrightarrow s_{ip} = 1,\ s_{in} = 0 \\ S_i = 0 \Leftrightarrow s_{ip} = 0,\ s_{in} = 0 \\ S_i = -1 \Leftrightarrow s_{ip} = 0,\ s_{in} = 1 \end{cases} \tag{5}$$

$$u_{Nn} = u_{S0} = \frac{1}{3} \sum_{i \in \{a,b,c\}} u_{Sin}, \tag{6}$$

$$u_{Si} = u_{Sin} - u_{S0}. \tag{7}$$

When regarding AC voltages referenced do the neutral point of the mains the Eqs. (6) and (7) are valid. Finally, DC side current of transistor-diode matrix may be calculated from (8).

$$i_{dcin} = \sum_{i \in \{a,b,c\}} i_{pi} = \sum_{i \in \{a,b,c\}} i_{ni} = \sum_{i \in \{a,b,c\}} \left[\frac{S_i + 1}{2}\,|S_i|\right] i_i + \\ + \sum_{i \in \{a,b,c\}} \left[(1 - |S_i|)\,\frac{sign\,(i_i) + 1}{2}\right] i_i. \tag{8}$$

The AC voltage of the converter represented in voltage space vector form is described by (9).

$$\mathbf{u}_{S\alpha\beta} = \mathbf{C}_{\mathbf{n}\to\alpha\beta} \begin{bmatrix} u_{San} \\ u_{Sbn} \\ u_{Scn} \end{bmatrix} = \mathbf{C}_{\mathbf{n}\to\alpha\beta} \begin{bmatrix} u_{Sa} \\ u_{Sb} \\ u_{Sc} \end{bmatrix} = \\ = \frac{u_{dc}}{2} \mathbf{C}_{\mathbf{n}\to\alpha\beta} \begin{bmatrix} S_a \\ S_b \\ S_c \end{bmatrix} + \\ + \frac{u_{dc}}{2} \mathbf{C}_{\mathbf{n}\to\alpha\beta} \begin{bmatrix} (1 - |S_a|) \cdot sign(i_a) \\ (1 - |S_b|) \cdot sign(i_b) \\ (1 - |S_c|) \cdot sign(i_c) \end{bmatrix}. \tag{9}$$

2. Control methods

Control system of VSC is realized by DSP and FPGA systems. For this nature it is typical discreet time system and one control period delay is characteristic for it. For this reason the problem of delay effect compensation is important for good converter controllability. To solve this problem, predictive-corrective control method is proposed. Model of converter system described in rotating reference frame (10) (Fig. 3) is useful for the purpose of control algorithm synthesis.

$$L\frac{d\underline{I}_{dq}}{dt} + R\underline{I}_{dq} + j\omega L\underline{I}_{dq} + \underline{V}_{Sdq} = \underline{V}_{dq}. \qquad (10)$$

This type of reference frame is useful for controlling of converter systems because of natural decoupling of controlled current components. Active and reactive current are controlled independently and in the case of sinusoidal time plots have value of constant in dq reference frame. A block diagram of control algorithm is illustrated in Fig. 4. Figure 5 presents the structure of the voltage space vector modulator system.

Novel converter systems are controlled by means of Digital Signal Processors and are systems with time quantization. For real systems with time quantization, the existence of time delay between measurement and control sequence generation is characteristic. It is due to analogy to digital conversion time and control algorithm execution time.

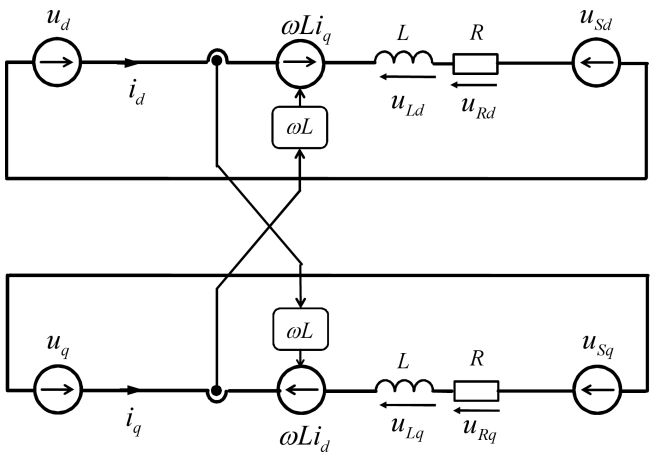

Fig. 3. Equivalent connection diagram of VSC in dq rotating reference frame

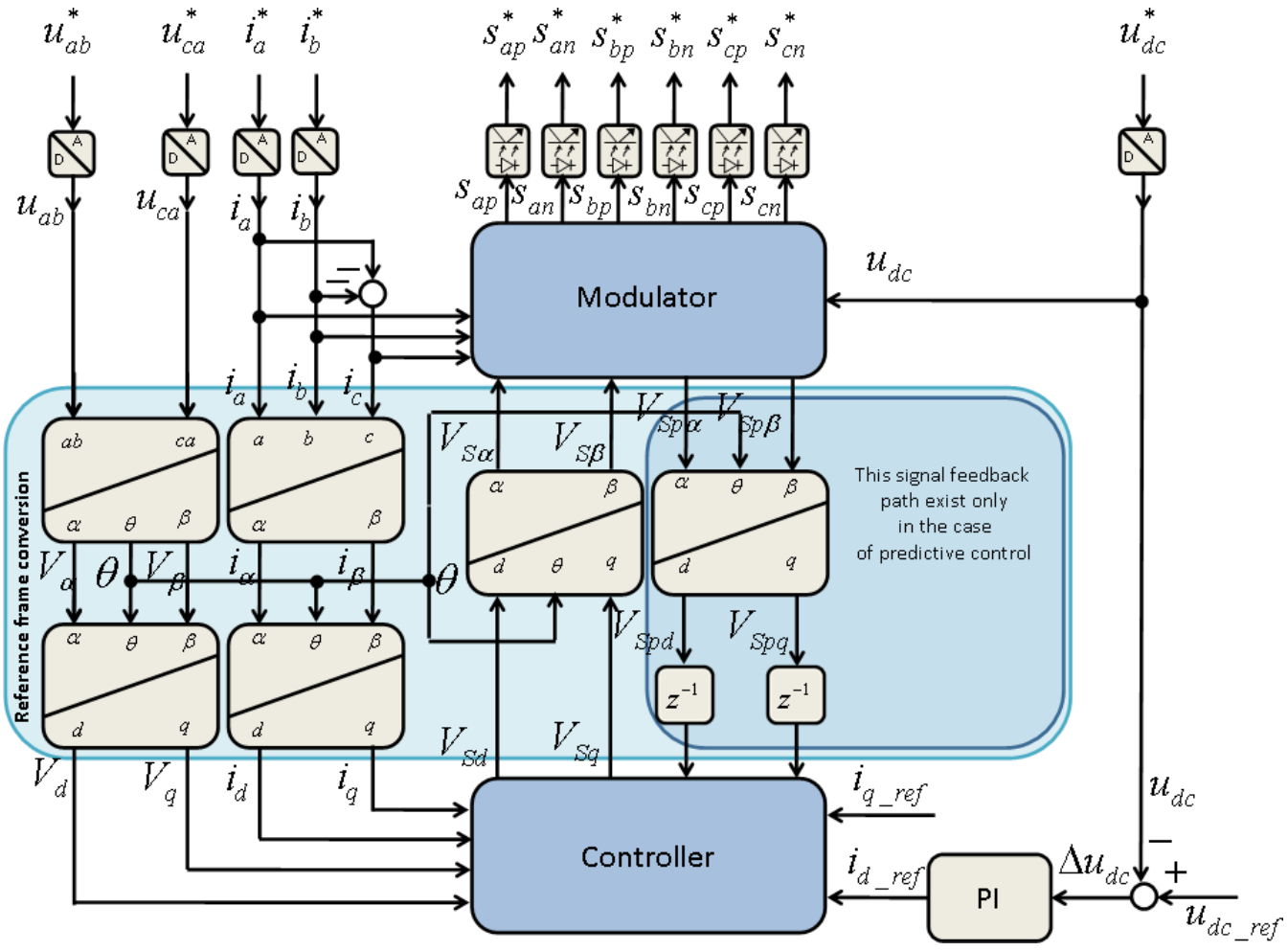

Fig. 4. Control system

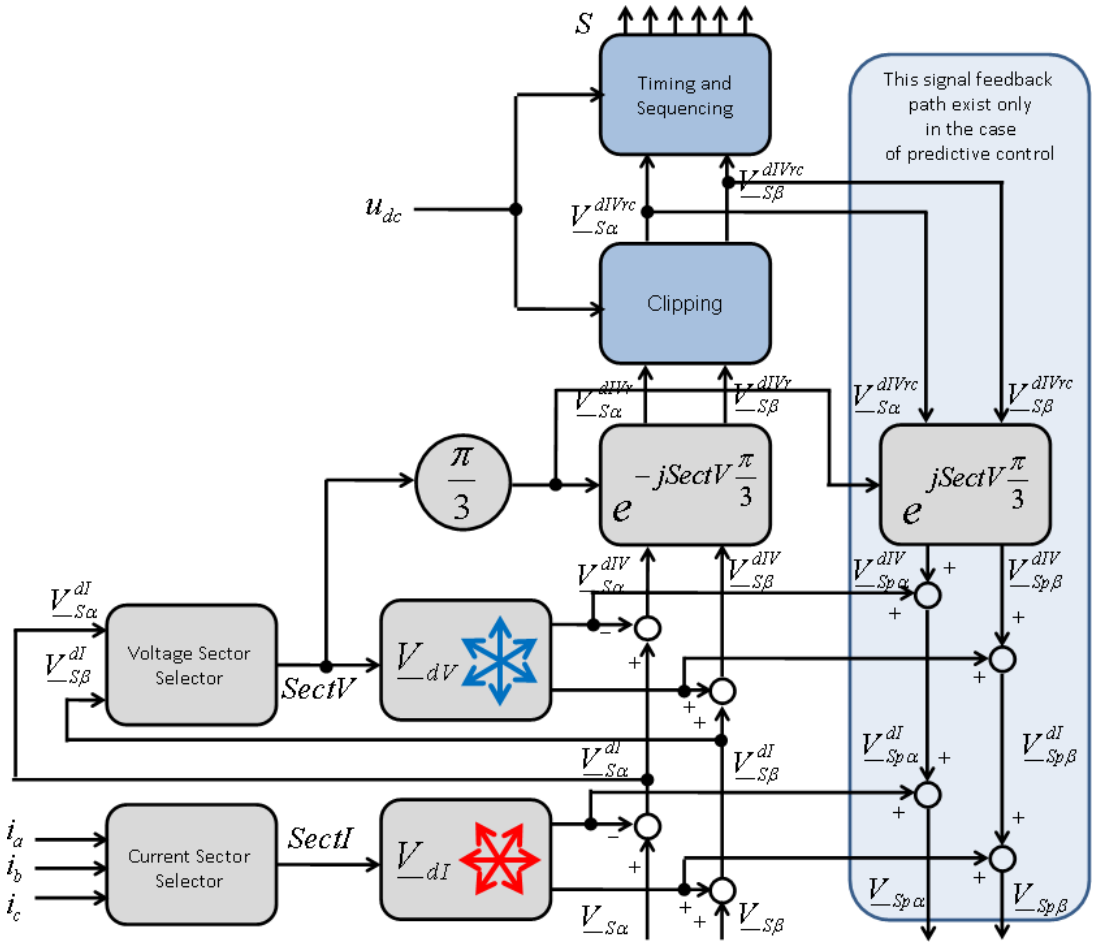

Fig. 5. Modulation system

2.1. Non-predictive control algorithm. In the case of non-predictive control algorithm, converter AC voltage for the next control step is calculated on the basis of current measurements. There is one control period delay between the measurements and applying of control sequence to converter switches. The voltage space vector for the next control step is calculated according to (11).

$$\underline{\mathbf{V}}_{S(i+1)dq} = \underline{\mathbf{V}}_{(i)dq} - (j\omega L + R)\,\underline{\mathbf{I}}_{(i)dq} - L\frac{\Delta\underline{\mathbf{I}}_{(i)dq}}{\mathrm{T}}, \quad (11)$$

$$\Delta\underline{\mathbf{I}}_{(i)dq} = \underline{\mathbf{I}}_{dq\,ref} - \underline{\mathbf{I}}_{(i)dq}. \quad (12)$$

For this reason the control sequence lags to voltages and currents of the mains. This situation leads to distortion of the converter phase currents.

2.2. Predictive-corrective control algorithm. To avoid current distortions caused by control delay prediction of control signals for the next control period is required. Figure 6 illustrates the principle of operation of predictive control algorithm in schematic way.

The time delay between sampling of currents and voltages and generating of new control sequence depending on these measurements is equal to the control period. For this reason the control algorithm takes into account only average values of voltage space vectors. This generally simplifies control algorithm synthesis.

The predictive-corrective control algorithm consists of two steps:

1. prediction of current that is generated by current voltage space vector that was calculated during previous control period,
2. calculation of the value of the voltage space vector that theoretically cancels current error in the next control step.

The predicted value of a converter current is described by Eq. (13).

$$\tilde{\underline{\mathbf{I}}}_{(i+1)dq} = \underline{\mathbf{I}}_{(\mathbf{i})dq} + \frac{1}{L}\left(\underline{\mathbf{V}}_{(\mathbf{i})dq} - \underline{\mathbf{V}}_{S(\mathbf{i})dq}\right)T - \\ -\frac{1}{L}\,(j\omega L + R)\,\underline{\mathbf{I}}_{(i)dq}T. \quad (13)$$

Converter voltage is counted on the basis on predicted value of converter current and mains voltage according to Eq. (14).

$$\underline{\mathbf{V}}_{S(i+1)dq} = \tilde{\underline{\mathbf{V}}}_{(i+1)dq} - (j\omega L + R)\,\tilde{\underline{\mathbf{I}}}_{(i+1)dq} - \\ -L\frac{\underline{\mathbf{I}}_{dq\,ref} - \tilde{\underline{\mathbf{I}}}_{(i+1)dq}}{\mathrm{T}}. \quad (14)$$

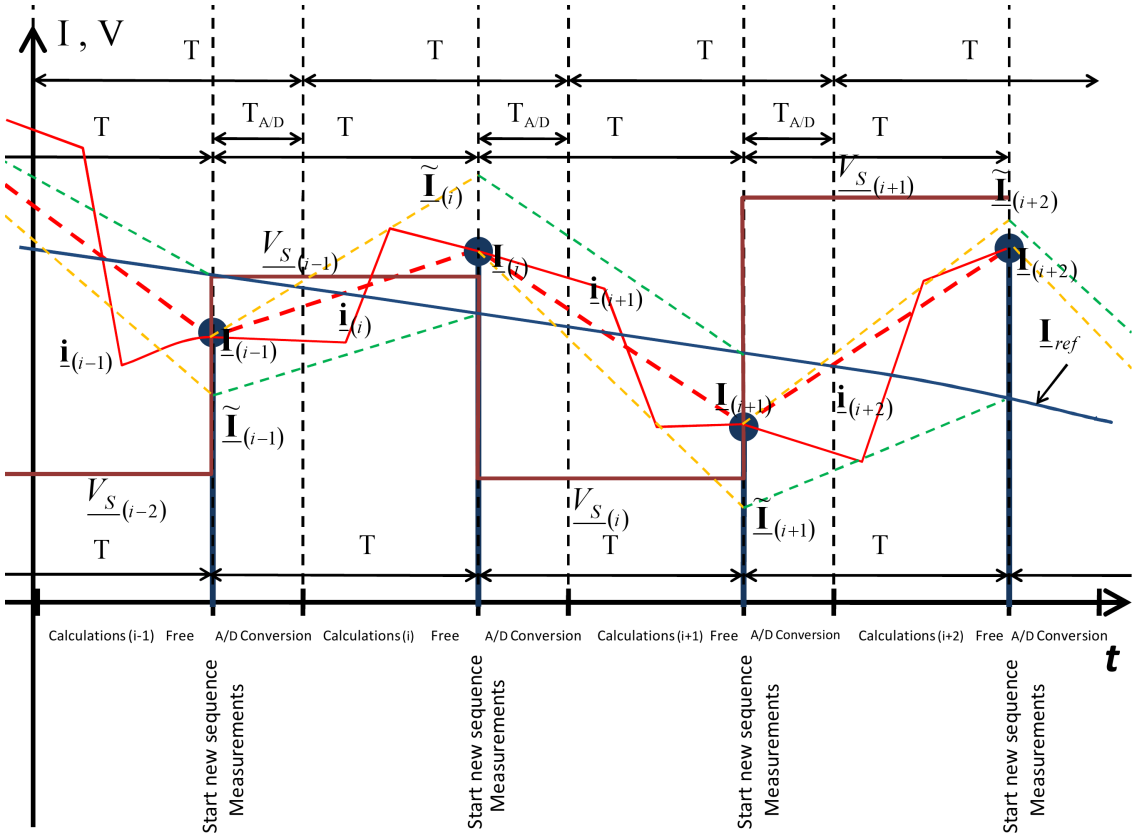

Fig. 6. Principle of operation of predictive-corrective control method

Mains voltage generally has stable value. It means that mains voltage is near sinusoidal and has near constant amplitude. Then it is a near constant vector in the synchronously rotated reference frame. This assumption is valid especially when considering value of mains voltage in two consecutive steps. For this reason Eqs. (15), (16) may be assumed. Then Eq. (14) takes form (17).

$$\tilde{\mathbf{V}}_{(i+1)\alpha\beta} = \mathbf{V}_{(i)\alpha\beta} e^{j\omega T}, \tag{15}$$

$$\tilde{\mathbf{V}}_{(i+1)dq} = \mathbf{V}_{(i)dq}, \tag{16}$$

$$\mathbf{V}_{S(i+1)dq} = \mathbf{V}_{(i)dq} - (j\omega L + R)\,\tilde{\mathbf{I}}_{(i+1)dq} - L\frac{\Delta\tilde{\mathbf{I}}_{(i+1)dq}}{\mathrm{T}}, \tag{17}$$

$$\Delta\tilde{\mathbf{I}}_{(i+1)dq} = \mathbf{I}_{dq\,ref} - \tilde{\mathbf{I}}_{(i+1)dq}. \tag{18}$$

Equation (13) together with (17) are the basis for control algorithm synthesis. The converter voltage (17) is calculated in the manner that predicted current regulation error (18), theoretically, should be cancelled after next control step. A prediction of current for the next step is based on the voltage space vector from previous step (13). For this reason a value of the common AC side voltage space vector, really applied to converter system, must be stored for the next control step. This function is realized by signal feedback path that is illustrated in control (Fig. 4) and modulation (Fig. 5) scheme. This path provides a voltage space vector clipped to effective modulation area to a predictive controller module.

3. Modulation methods

The existence of a dead time in the modulation sequence causes that an effective voltage space vector modulation area is restricted (Fig. 8). Regions outside the sector outline are inaccessible [8]. The effective modulation areas may be converted into one coherent area corresponding to the operation of the converter outside dead time periods [8] (Fig. 10). This converted area is obtained by shifting restricted operation regions by voltage space vector shift vectors. The overall shift vector (19) has two component vectors, one dependent on current sector (20), (22) and second on voltage one (21), (23) [8] (Fig. 9).

$$\underline{V_d} = \underline{V_{dI}} + \underline{V_{dV}}, \tag{19}$$

$$\underline{V_{dI3}} = 2\sqrt{\frac{2}{3}}\frac{T_d}{T} u_{dc} e^{jSectI\frac{\pi}{3}}, \tag{20}$$

$$\underline{V_{dV3}} = 2\sqrt{2}\frac{T_d}{T} u_{dc} e^{j\left(SectV+\frac{1}{2}\right)\frac{\pi}{3}}, \tag{21}$$

$$\underline{V_{dI4}} = 2\sqrt{\frac{2}{3}}\frac{T_d}{T} u_{dc} e^{jSectI\frac{\pi}{3}}, \tag{22}$$

$$\underline{V_{dV4}} = \sqrt{6}\frac{T_d}{T} u_{dc} e^{jSectV\frac{\pi}{3}}. \tag{23}$$

a) SVPWM3

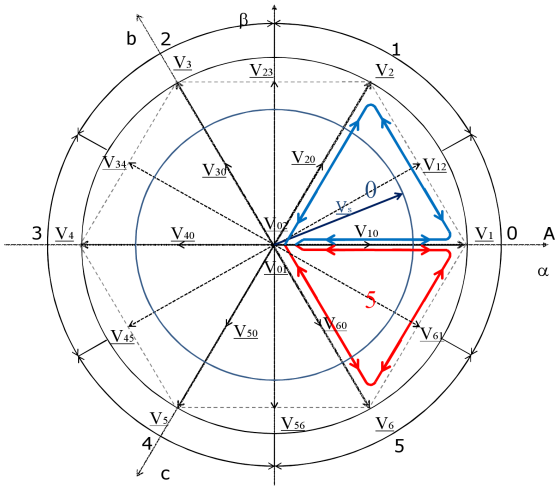

$SectV = 0$; sequence: $V_{01}, V_1, V_2, V_{02}, V_2, V_1, V_{01}$

b) SVPWM4

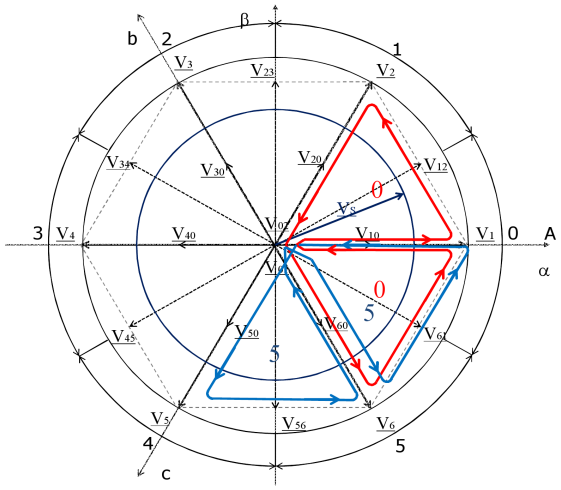

$SectV = 0$; sequence: $V_{02}, V_6, V_1, V_{01}, V_1, V_2, V_{02}$

Fig. 7. Voltage space vector sequencing

a) SVPWM3

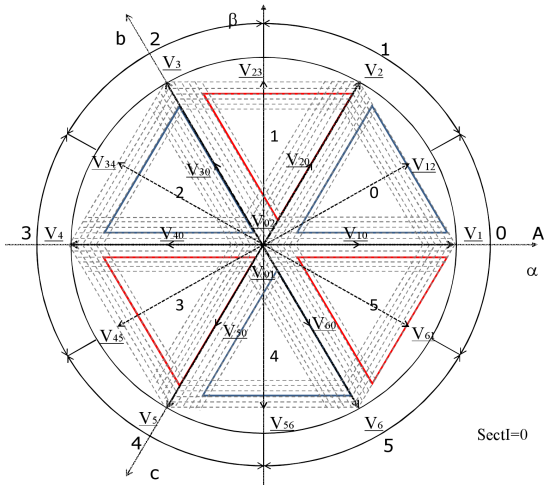

b) SVPWM4

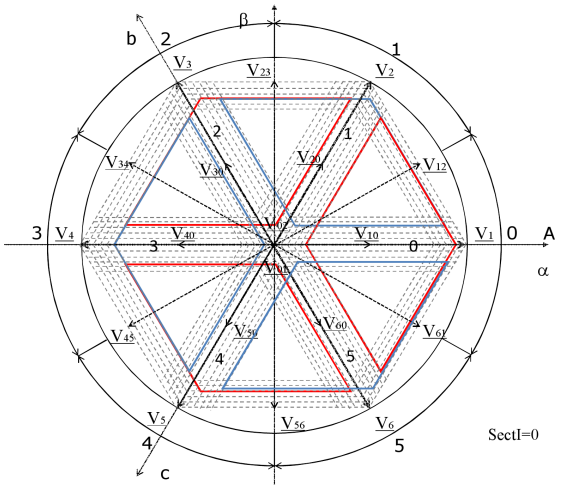

Fig. 8. Voltage space vector pulse width modulation area for current sector 0

a) SVPWM3

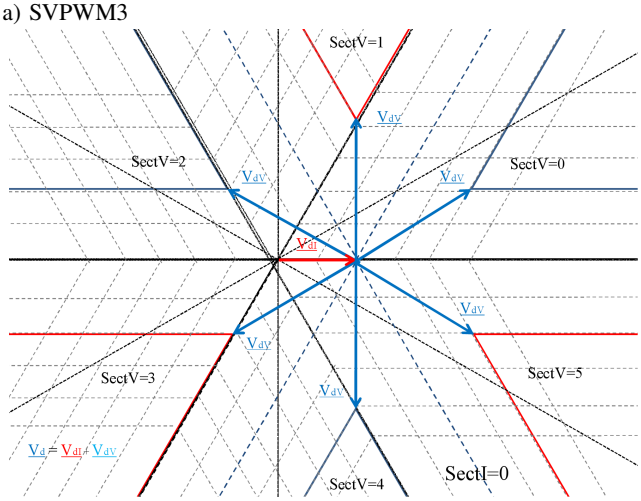

b) SVPWM4

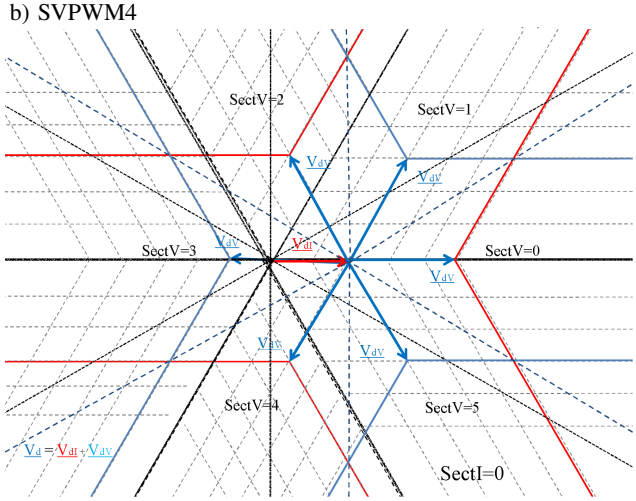

Fig. 9. Voltage space vector pulse width modulation area (surroundings of coordinate origin) for current sector 0

a) SVPWM3 b) SVPWM4

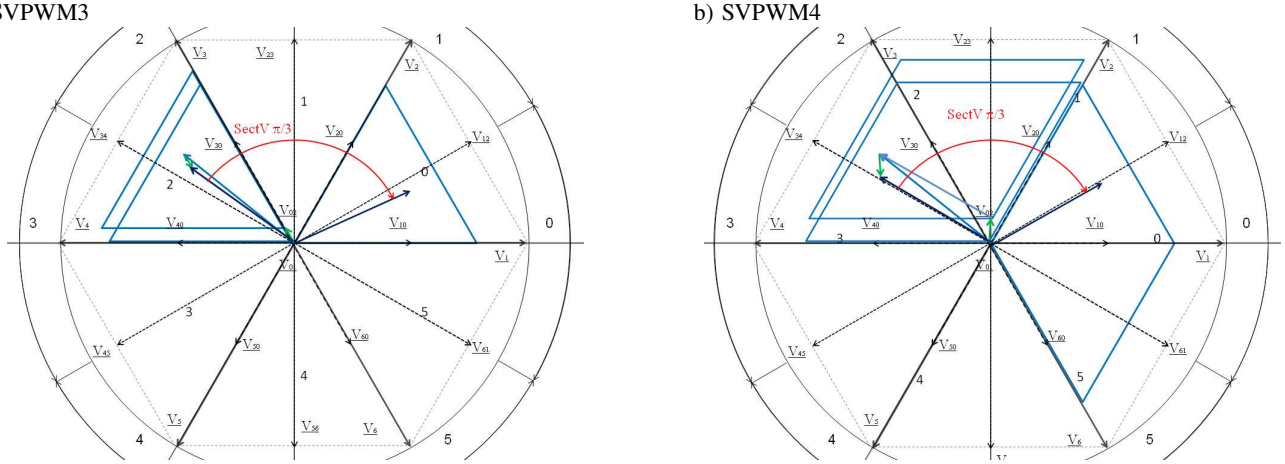

Fig. 10. Voltage space vector modulation area transformation

a) SVPWM3 b) SVPWM4

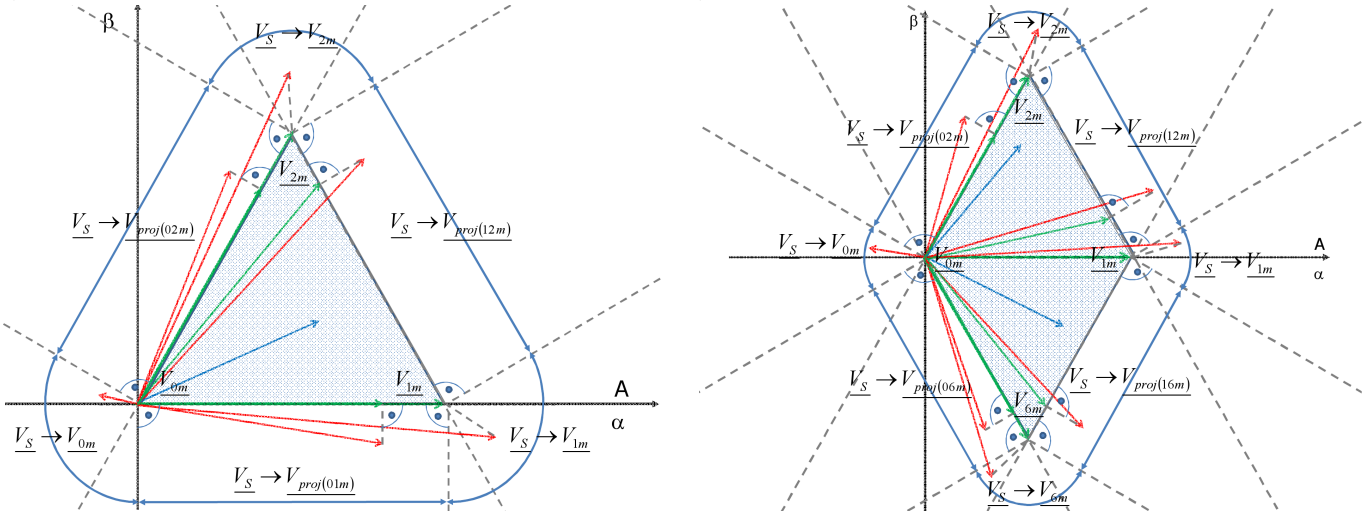

Fig. 11. The principle of Voltage space vector clipping operation

a) SVPWM3: $SectI = 0$; $SectV = 0$ b) SVPWM4: $SectI = 0$; $SectV = 0$

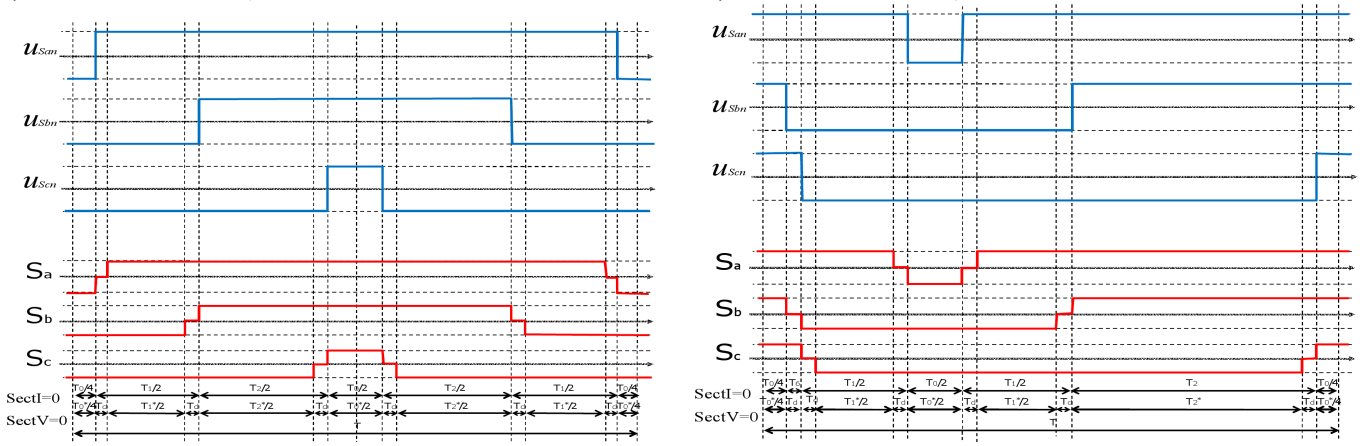

Fig. 12. Voltage space vector pulse width modulation time plots of converter voltages and branch state functions

Figures 7a and 7b present basic voltage space vector sequencing for SVPWM3 and SVPWM4 modulation methods [8].

Due to implemented sequence the effective areas of voltage space vector modulation for zero current sector are illustrated in Fig 8. In the case of SVPWM3 method the areas related to different voltage sectors are incoherent. There are gaps between them even for small values of dead time. For method SVPWM4 this situation may occur only in the case of an extremely large dead time value. In typical control situations effective modulation areas overlap with each other and create a coherent area of modulation.

In the proposed modulation method a first current sector number is calculated. On the basis of the current sector number the end of the commanded voltage space vector is shifted by vector $\underline{V_{dI}}$ (20), (22). Then voltage sector is calculated. The end of commanded voltage space vector is shifted by the vector $\underline{V_{dV}}$ (21), (23). The resulting voltage space vector is rotated by an angle of $-SectV\pi/3$ to the zero current sector. This rotation is made in order to simplify the vector projection and calculation of times of the basic voltage space vector switch on. Then the voltage space vector is constrained to the effective modulation area (Fig. 11).

$$\underline{V_{Sp}} = \underline{V_{SpdI}} + \underline{V_{dI}}, \tag{24}$$

$$\underline{V_{SpdI}} = \underline{V_{SpdIV}} + \underline{V_{dV}}. \tag{25}$$

In the case of the predictive-corrective control algorithm the constrained voltage space vector is reversibly converted and used in the next control step (signal feedback path in Fig. 4 and Fig. 5), (24), (25).

3.1. Constrains of voltage space vector modulation area. In situation when voltage space vector end is located outside the effective modulation area the clipping algorithm must be performed. The principle of clipping operation for both modulation method are illustrated in Fig. 11. There are regions (denoted by bow arrows) where voltage space is clipped to vertex vector and regions (marked by line arrows) where voltage space vector is clipped to its projection on the modulation area edge. It guaranties that voltage space vector difference between the commanded vector and its real realisation is the smallest as possible.

4. Test conditions

Simulation and experimental investigation were made for the next conditions: $L = 10$ mH, $R \approx 0.1\Omega$, $C = 1100\ \mu F$, $R_o = 350\ \Omega$, $f = 50$ Hz($\omega = 314.15$ rad/s), $U_{RMS} = 81.6$ V, $THD(u) = 0\%$ (for simulation only), $THD(u) = 3\%$ (for simulation and experiment), $T = 100\ \mu s$, $T_d = 2\ \mu s$. In simulation, it was assumed that converter parameters and parameters of controller model have values of equal to each other.

5. Simulations

Figures 13 and 14 present simulation results for SVPWM3 (Fig. 13) and SPWM4 (Fig. 14) modulation methods in the case of $THD(u) = 0\%$ and non-predictive control method.

Figures 15 and 16 present simulation results for SVPWM3 (Fig. 15) and SPWM4 (Fig. 16) modulation methods in the case of $THD(u) = 0\%$ and predictive control method.

Figures 17 and 18 present simulation results for SVPWM3 (Fig. 17) and SPWM4 (Fig. 18) modulation methods in the case of $THD(u) = 3\%$ and non-predictive control method.

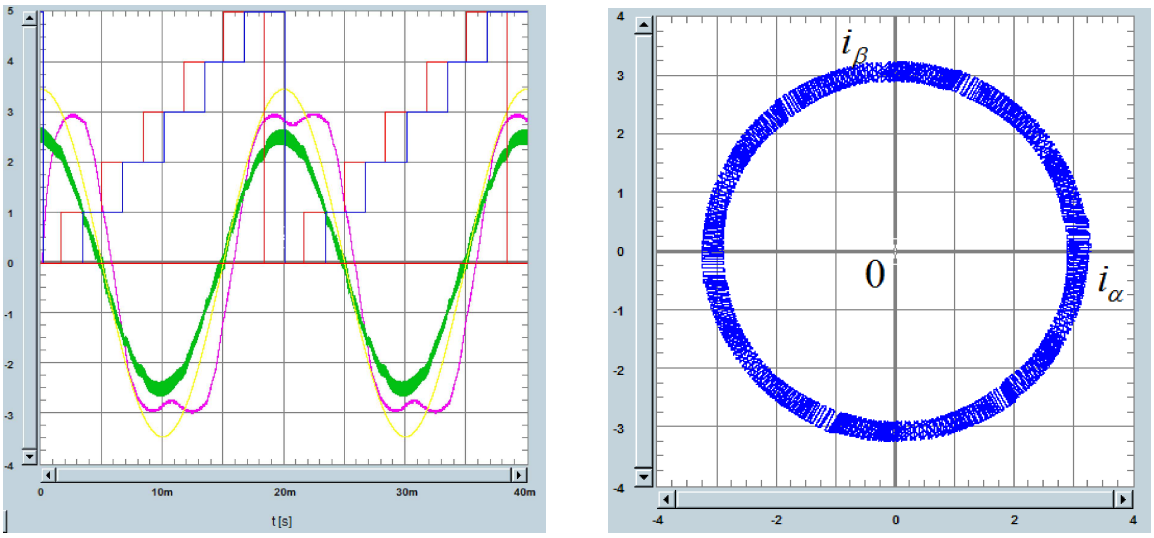

Fig. 13. Simulation of VSC controlled by non-predictive control method and SVPWM3 modulation method

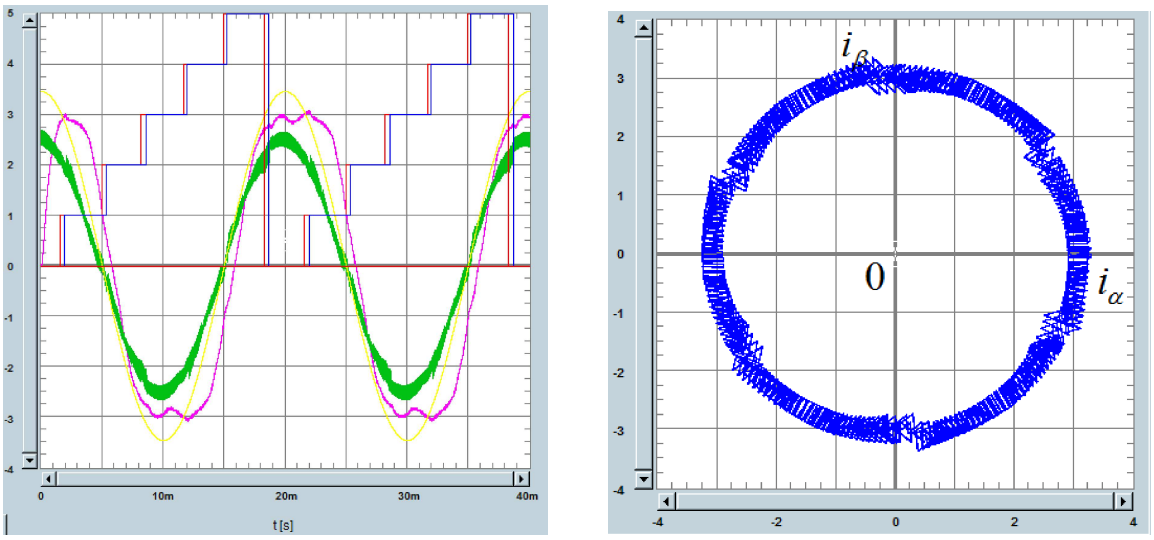

Fig. 14. Simulation of VSC controlled by non-predictive control method and SVPWM4 modulation method

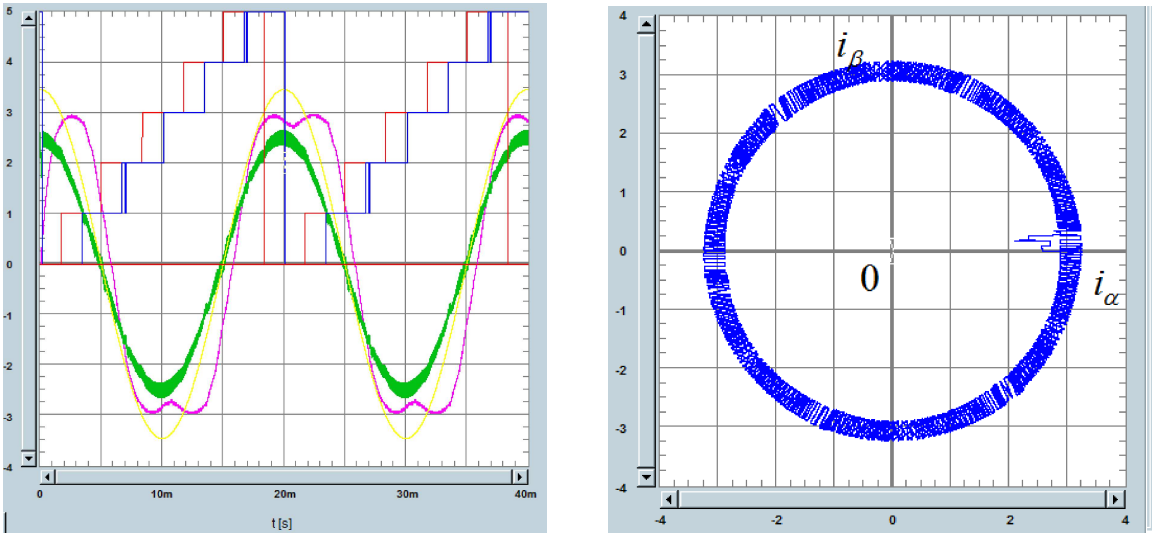

Fig. 15. Simulation of VSC controlled by predictive control method and SVPWM3 modulation method

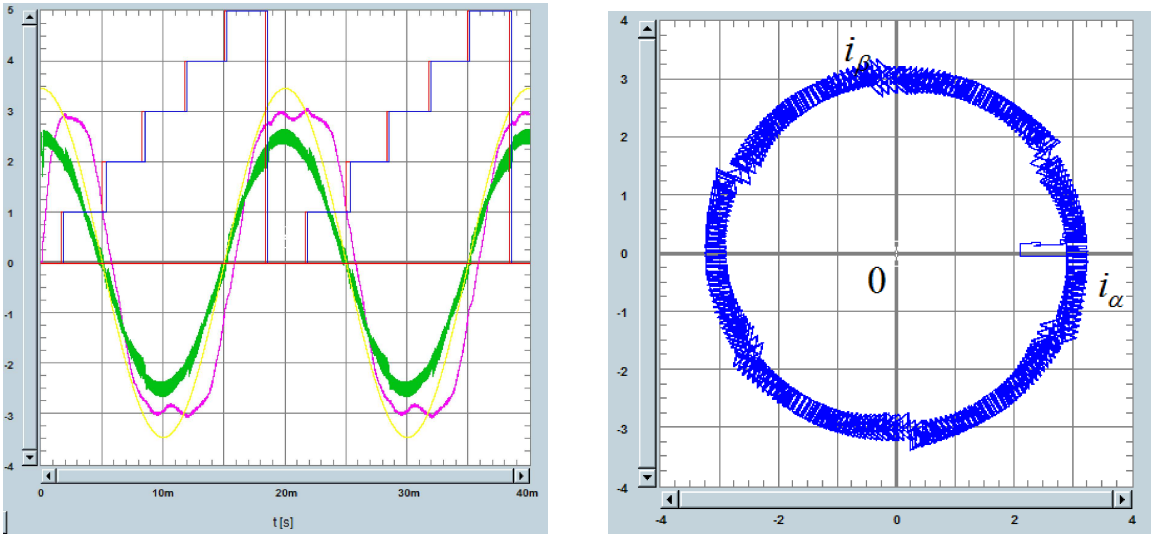

Fig. 16. Simulation of VSC controlled by predictive control method and SVPWM4 modulation method

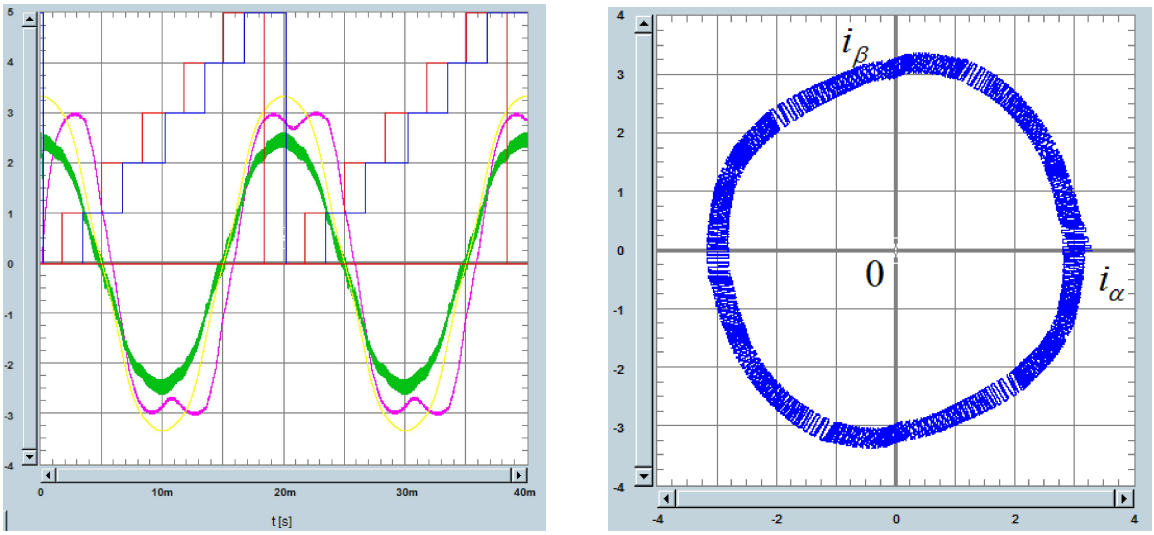

Fig. 17. Simulation of VSC controlled by non-predictive control method and SVPWM3 modulation method

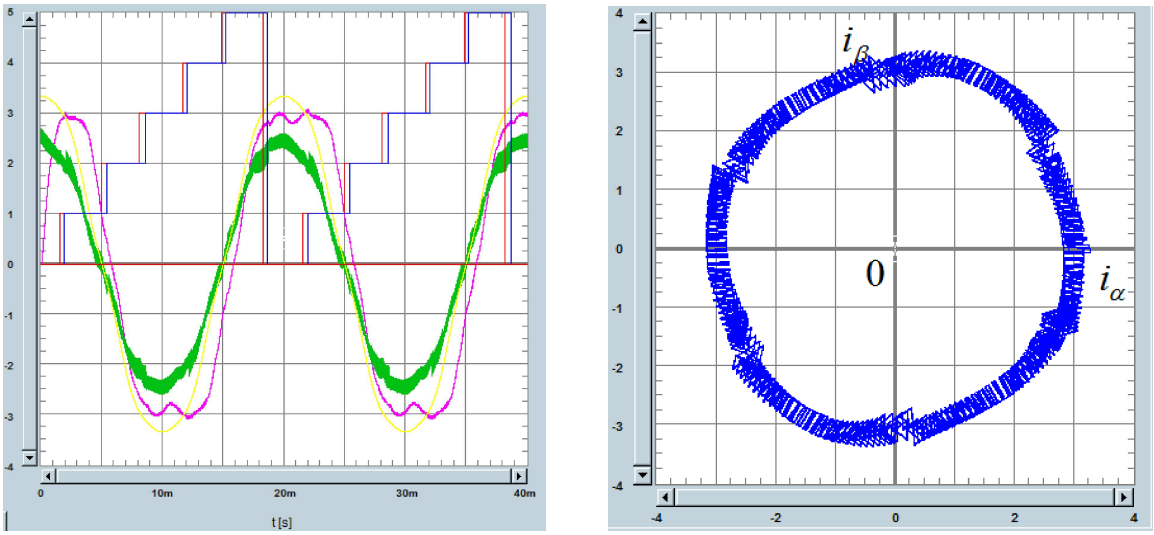

Fig. 18. Simulation of VSC controlled by non-predictive control method and SVPWM4 modulation method

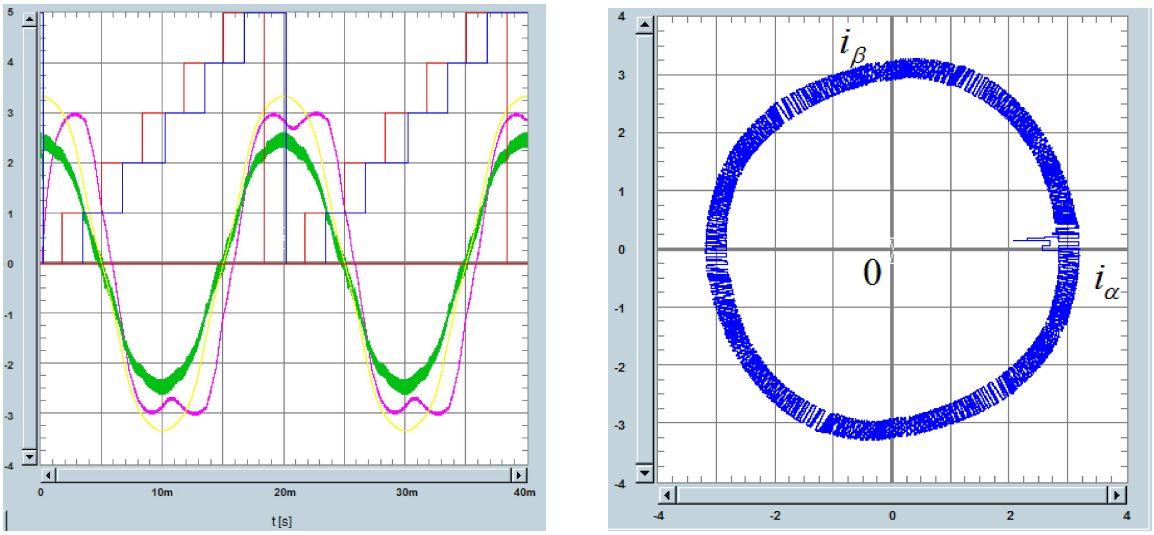

Fig. 19. Simulation of VSC controlled by predictive control method and SVPWM3 modulation method

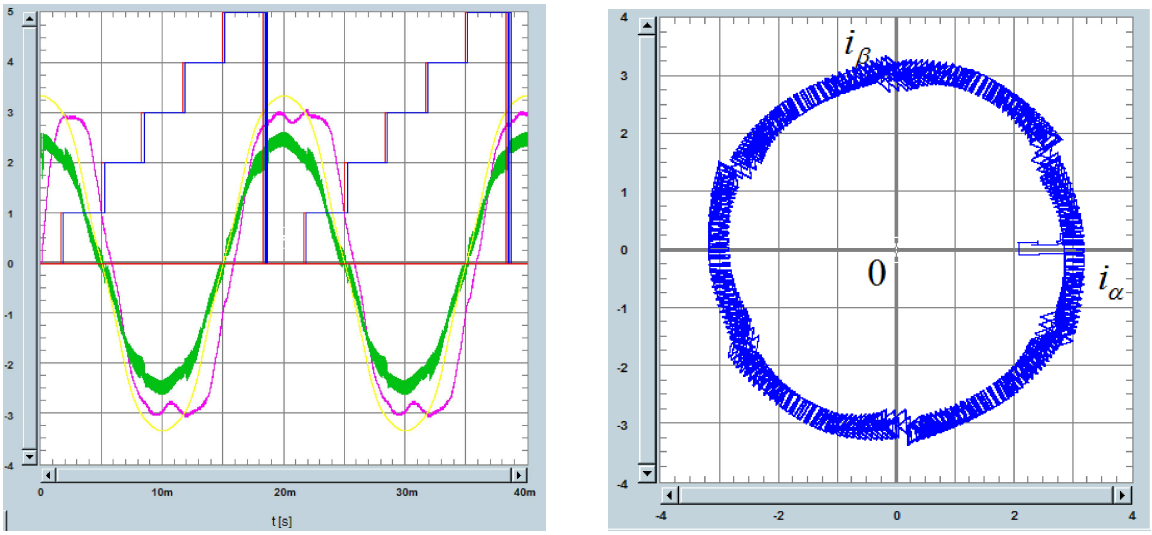

Fig. 20. Simulation of VSC controlled by predictive control method and SVPWM4 modulation method

Figures 19 and 20 present simulation results for SVPWM3 (Fig. 19) and SPWM4 (Fig. 20) modulation methods in the case of $THD(u) = 3\%$ and predictive control method.

From the analysis of simulation results it can be seen that in both cases of SVWM3 and SVPWM4 method there are current distortions at the voltage sectors boundary. But current distortions have different sources. In the case of SVPWM3 method they are caused by impossibility of the voltage space vector realisation due to gaps of effective voltage space vector area. In the case of SVPWM4 method they are concerned with a change of direction of basic voltage space vectors sequencing in modulation sequence.

6. Experimental investigations

The laboratory setup was constructed to validate proposed control and modulation algorithm. The view of laboratory setup is illustrated in Fig. 21 and Fig. 22.

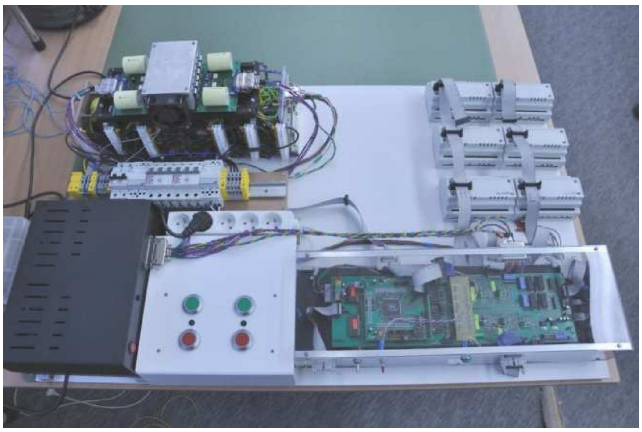

Fig. 21. Experimental setup of VSC

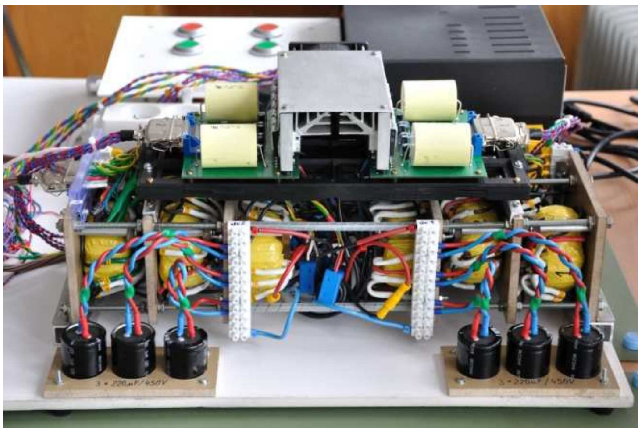

Fig. 22. Power converter part

Both control methods (non-predictive and predictive) in conjunction with both modulation method (SVWM3 and SVPWM4) were realised. Figures 23 and 24 present selected time plots of control and modulation system for SVPWM3 modulation method.

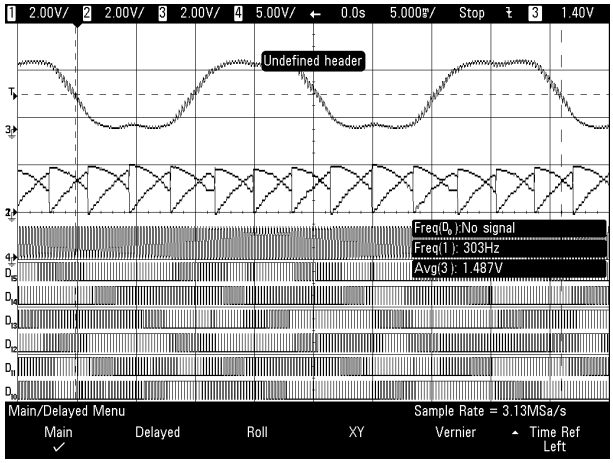

Fig. 23. Control and modulation signals – SVPWM3

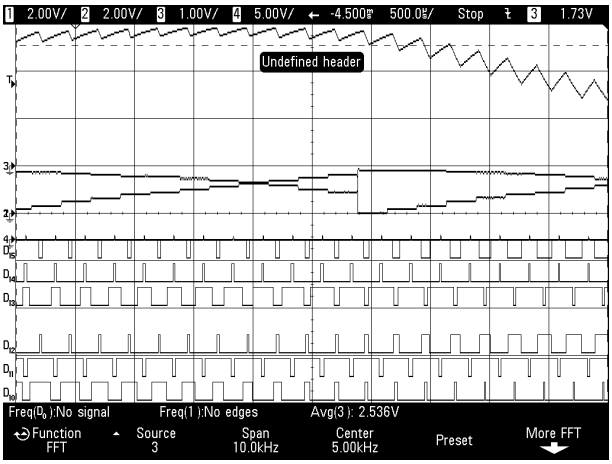

Fig. 24. Control and modulation signals – SVPWM3

Respective time plots for SVPWM4 modulation method are illustrated in Fig. 25 and 26.

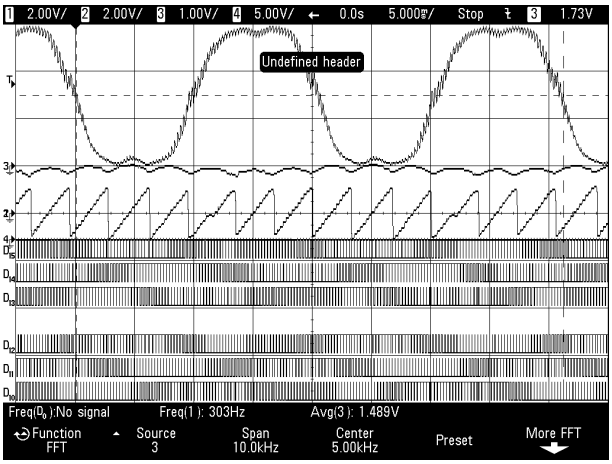

Fig. 25. Control and modulation signals – SVPWM4

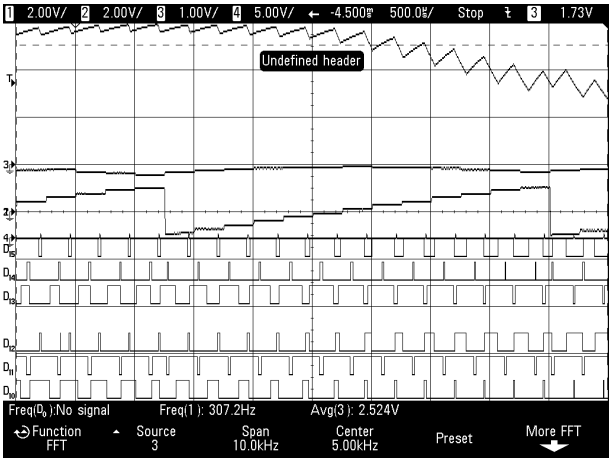

Fig. 26. Control and modulation signals – SVPWM4

Phase current and its spectrum acquired in the case of the control algorithm switched off are illustrated in Fig. 27 and 28.

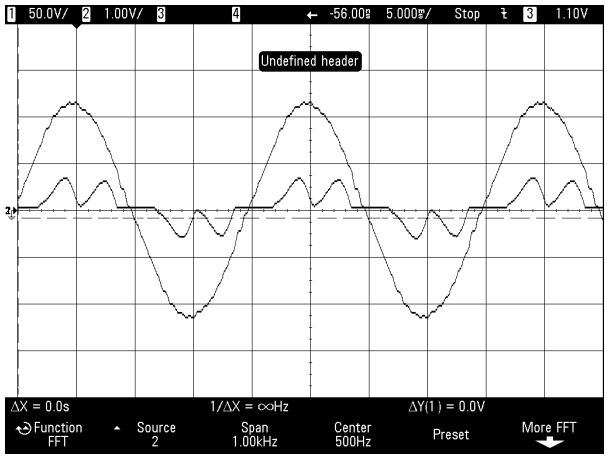

Fig. 27. Phase current and voltage in the case of control algorithm switched off

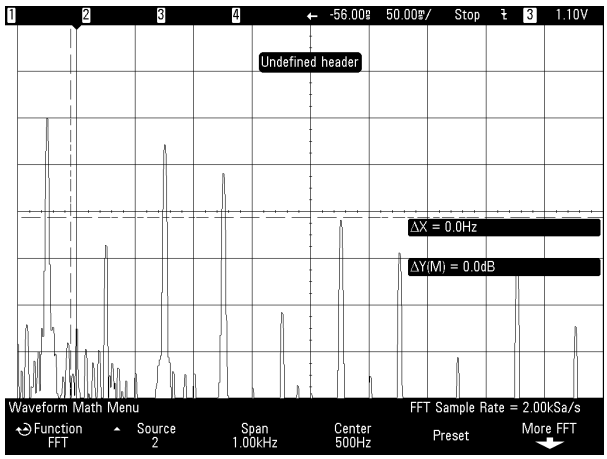

Fig. 28. Current spectrum (10dBV/div 100Hz/div) in the case of control algorithm switched off

All transistors are switched off, only a diode rectifier functions. These plots are published as a base for comparison of power quality improvement. The work of VSC system with near unity power factor for non-predictive control mode is presented in Fig. 29. Figure 30 illustrates current spectrum. Supply AC voltage was distorted and had THD value about of 3%.

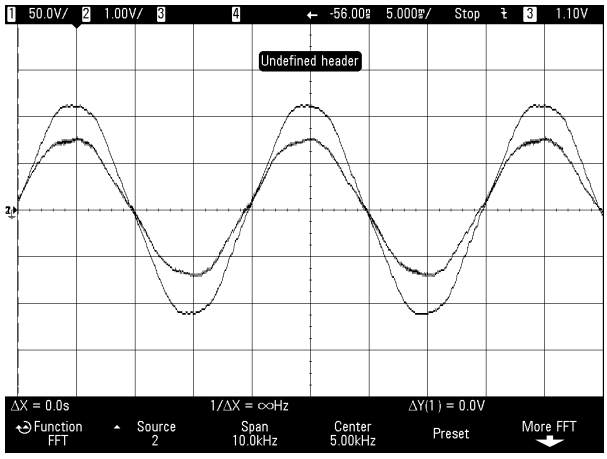

Fig. 29. Phase current and voltage – non-predictive control, SVPWM3, near unity power factor

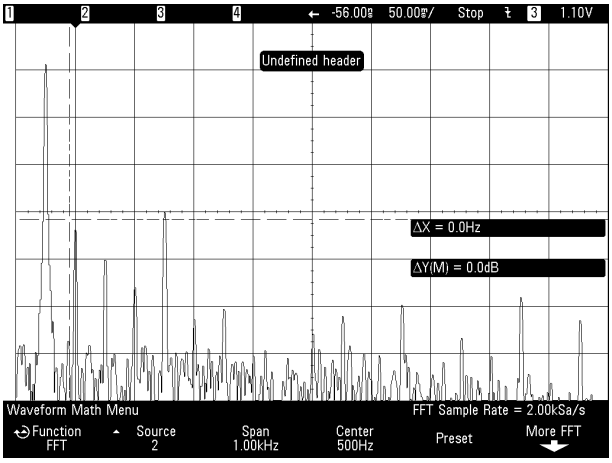

Fig. 30. Current spectrum (10 dBV/div 100 Hz/div) – non-predictive control, SVPWM3, near unity power factor

Also a work of the VSC system with additional capacitive reactive power was examined (Fig. 31 and 32).

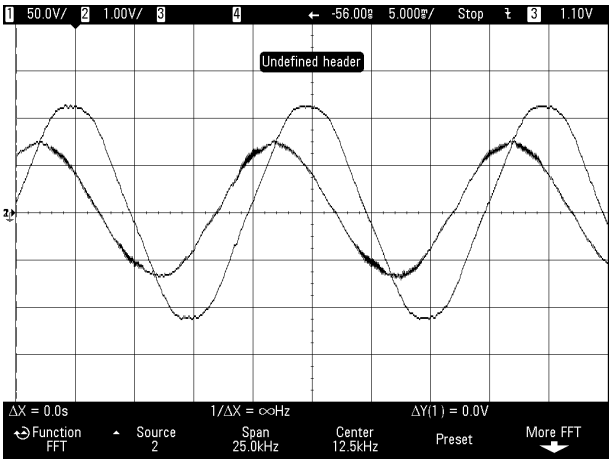

Fig. 31. Phase current and voltage – non-predictive control, SVPWM3, capacitive power factor

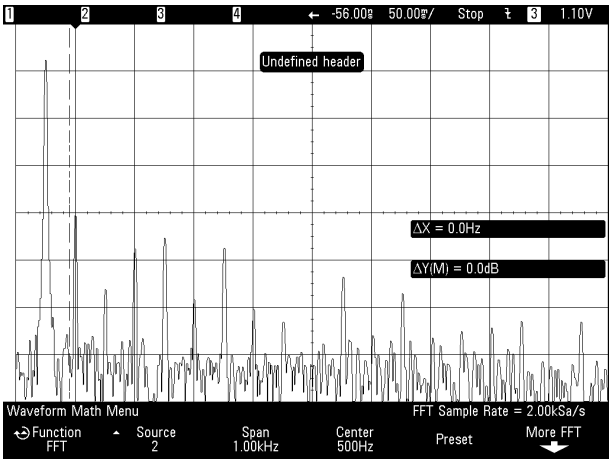

Fig. 32. Current spectrum (10 dBV/div 100 Hz/div) – non-predictive control, SVPWM3, capacitive power factor

To obtain less distorted current the prediction-correction control algorithm was implemented. Figures 33 and 34 illustrate phase current and voltage time plots and current spectrum measured in VSC system working with near unity power factor.

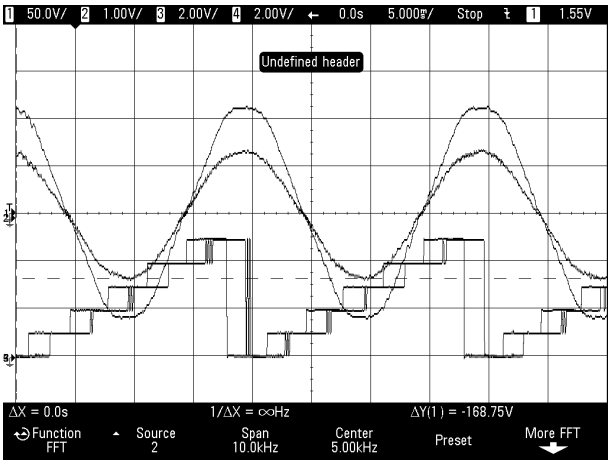

Fig. 33. Phase current and voltage - predictive control, SVPWM3, near unity power factor

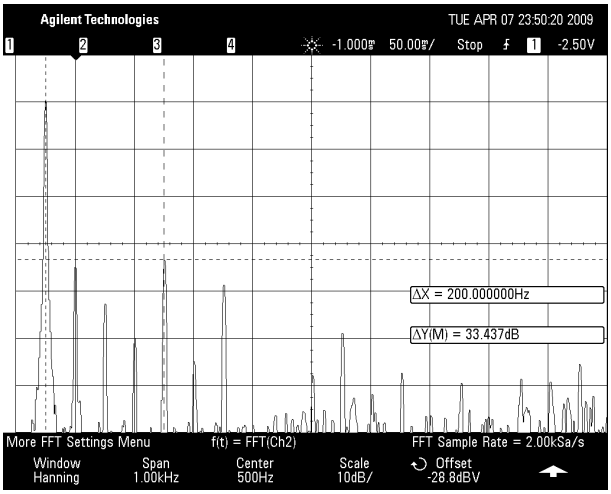

Fig. 34. Current spectrum (10 dBV/div 100 Hz/div) - predictive control, SVPWM3, near unity power factor

In the case of predictive control method phase current is less distorted than in the case of non-predictive control. Distance between fundamental current harmonic and the largest higher harmonic is about of 31 dB in the case of non-predictive control and about 33 dB in the case of predictive control for system works with near unity power factor. Time plots of phase current and voltage acquired for work of VSC with additional capacitive power for predictive control method are illustrated in Fig. 35. Figure 36 presents transition from work with additional inductive power to work with capacitive one.

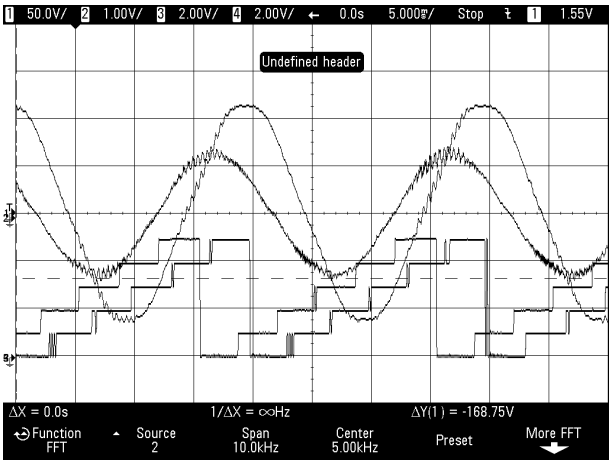

Fig. 35. Phase current and voltage – predictive control, SVPWM3, capacitive power factor

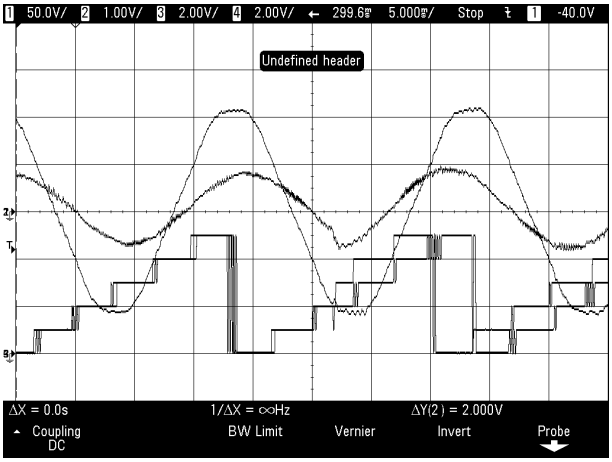

Fig. 36. Transition from the work with inductive reactive power to work with capacitive reactive power - predictive control, SVPWM3

7. Conclusions

The paper provides details of VSC modelling, controlling and modulation. VSC is modelled with utilization of three value transistor branch state function [8]. The predictive control method for VSC is developed. New modified voltage space vector modulation methods that base on the introduced VSC model are proposed [8]. Correctness of the proposed methods is proven by simulations and experimental investigations. Simulation give similar results for non-predictive and predictive control method in the same and other conditions. A representative set of experimental time plots illustrating converter work in different modes and acquired current spectrums are published. From the experimental results the predictive method seems to be better than the non-predictive due to less level of high harmonic distortion. For the work of converter system with near unity power factor the high total power factor value of $TPF \approx 0.995$ and low total harmonic distortion value of $THD(i) \approx 3\%$ for mains harmonic distortion value of $THD(u) \approx 3\%$ was obtained.

References

[1] J. Holtz, "Pulsewidth modulation – a survey", *IEEE Transactions on Industrial Electronics* 39 (5), 410–420 (1992).

[2] H. Pinheiro, F. Botterón, C. Reh, L. Schuch, R.F. Camargo, H.L. Hey, H.A. Grundling, and R.J. Pinheiro, "Space vector modulation for voltage-source inverters: a unified approach", *IECON 02* 1, 5–8 (2002).

[3] P. Antoniewicz and M.P. Kaźmierkowski, "Predictive direct power control of three-phase boost rectifier", *Bull. Pol. Ac.: Tech.* 54 (3), 287–292 (2006).

[4] M. Malinowski, "Sensorless control strategies for three-phase PWM rectifiers", *Ph.D. Thesis*, Warsaw University of Technology, Warsaw, 2001.

[5] M. Jasiński, "Direct power and torque control of ac/dc/ac converter-fed induction motor drives", *Ph.D. Thesis*, Warsaw University of Technology, Warsaw, 2005.

[6] R. Strzelecki and H. Supronowicz, "Power coefficient in AC power supply systems and ways of its improvement", Publishing House of the Warsaw University of Technology, Warsaw, 2000, (in Polish).

[7] L. Chen and F.Z. Peng, "Dead-time elimination for voltage source inverters", *IEEE Transactions on Power Electronics* 23 (2), 574–580 (2008).

[8] G. Radomski, „Modelling and modulation of voltage source converter", *13th Int. Power Electronics and Motion Control Conf.* 1, 504–511 (2008).